IEEE Access
Multidisciplinary | Rapid Review | Open Access Journal

Received 19 March 2024, accepted 18 April 2024, date of publication 23 April 2024, date of current version 3 May 2024.

Digital Object Identifier 10.1109/ACCESS.2024.3392796

RESEARCH ARTICLE

Concealment of Chaos Time Delay Signature in a Ring Network With Heterogeneous Delays Based on Nano-Lasers

XUETING ZHANG[1], PENGHUA MU[1], (Member, IEEE), YIQIAO WANG[1], GANG GUO[2], XINTIAN LIU[2], AND XIA LIU[1]

[1]School of Opto-Electronic Information Science and Technology, Yantai University, Yantai, Shandong 264003, China
[2]Yuweng Information Technology Company Ltd., Weihai 264210, China

Corresponding authors: Penghua Mu (ph_mu@ytu.edu.cn) and Xia Liu (ytuliuxia@ytu.edu.cn)

This work was supported in part by the Natural Science Foundation of Shandong Province under Project ZR2020QF090; in part by the Key Laboratory of Modern Optical Technologies of the Education Ministry of China, Soochow University, under Grant KJS2066; and in part by the Key Laboratory of Advanced Optical Manufacturing Technologies of Jiangsu Province, Soochow University, under Grant KJS2045.

ABSTRACT In this paper, we numerically investigate the concealing properties of time delay signature (TDS) in the chaotic output of a ring network composed of three mutually coupled semiconductor nano-lasers, comparing the TDS evolution between a ring network with identical coupling delays and a ring network with heterogeneous coupling delays. In simulations, an autocorrelation function is introduced to assess the system's capability in concealing the TDS. By examining the impacts of system parameters such as coupling strength, frequency detuning, Purcell factor F, spontaneous radiation coupling factor β, and bias current I on the concealment of TDS, we identify the parameter ranges that successfully conceal TDS. The findings indicate that, compared to ring networks featuring identical coupling delays, those with heterogeneous delays can conceal TDS over a broader parameter range. Additionally, F moderately and β relatively small can expand the region of TDS concealment, while the influence of I on TDS is relatively negligible in the ring network with heterogeneous delays.

INDEX TERMS Nano-lasers, time delay signature, heterogeneous delays.

I. INTRODUCTION

With the exposure of information security issues, there has been widespread concern about the enhancement of security in optical communication systems. It is well known that optical chaos sources are an ideal choice for chaotic secure communication [1], [2], [3] and physical random number generators [4], [5], [6]. Among others, the generation of chaotic laser signals can be generated through a variety of methods, broadly categorized as optical feedback [7], optical injection [8], optoelectronic feedback [9], and current modulation [10], etc. In any of these additional degrees of freedom, semiconductor lasers (SLs) can efficiently produce high-dimensional, wide-bandwidth, and complex chaotic outputs. In particular, in most schemes based on SLs to generate chaotic signals, delay self-feedback or delay coupling is often employed to produce chaotic signals with large bandwidth as well as high unpredictability. However, it is noteworthy that these systems exhibit a certain degree of periodicity, known as time delay signatures (TDS). Currently, TDS can be extracted utilizing time series analysis techniques, including autocorrelation function (ACF), permutation entropy (PE), and delay mutual information (DMI) [11], [12], [13]. If chaotic signals with TDS are used as information carriers, the risk of information leakage related to key parameters will increase. By extracting time delay information, eavesdroppers can acquire key parameters of the communication system, allowing them to reconstruct the chaotic secure system. This poses a threat to the security of chaotic communication systems [14]. Simultaneously, the

The associate editor coordinating the review of this manuscript and approving it for publication was Chao Zuo.

incorporation of TDS also degrades the randomness performance of random number generators [15]. Hence, improving the quality of chaotic signals (hiding the system's TDS) is a hot topic of attention for many scholars.

In the existing research, most schemes for implementing TDS concealment are primarily focused on single SL or coupling systems composed of only two SLs [16], [17], [18], [19], [20], [21]. For instance, Wu et al. conducted experimental and numerical analyses to show that the SL system with dual optical feedback can achieve TDS suppression in chaotic output [17]. Subsequently, Wu et al. further investigated TDS in mutually delayed coupled SL systems, revealing that this system can conceal TDS better, and suppressing all TDS to the level of background noise [18]. Additionally, Mu et al. mainly explored TDS of master-slave injection systems with phase-conjugate feedback (PCF), to illustrate this advantage, a master-slave injected system with optical feedback (COF) was chosen for comparison. The simulation results suggest that, in comparison to the COF system, the PCF system can achieve TDS concealment over a larger range [19]. Furthermore, owing to the potential applications of SL networks in chaotic communication networks and random number generation, the chaotic synchronization behaviors and unpredictability in networks of SLs have been extensively studied [22], [23], [24], [25], [26]. However, the evolution of TDS in ring networks is still not fully explored [27], [28], [29], especially in the case of TDS evolution in ring networks composed of nano-lasers (NLs).

This is because the aforementioned studies have all employed traditional SLs, and to overcome the bottleneck of large size for future large-scale integration, it is necessary to explore beyond the limitations of traditional SLs. The NLs possess characteristics such as small size, low power consumption, and fast response, making them promising for applications in photonic integrated circuits (PICs). Therefore, they have attracted significant attention in recent years. Scholars have proposed various theoretical models of semiconductor NLs to study their dynamic characteristics [30], [31], [32], [33], [34], [35], [36], [37], [38], [39] and TDS concealment [40], [41], [42]. Among them, the TDS concealment mechanism in ring networks based on NLs has not been explored. Hence, it is meaningful to investigate the evolution of TDS in chaotic signals within ring networks based on NLs in order to ascertain if such systems can provide novel functionalities within the framework of PICs.

The purpose of the paper is to achieve hiding of TDS in a ring network featuring heterogeneous coupling delays. For comparative analysis, the TDS characteristics of a ring network featuring identical coupling delays are provided. Across the entire work, the RNI network denotes three NLs mutually coupled featuring identical coupling delays, whereas the RNH network represents three NLs mutually coupled featuring heterogeneous coupling delays. The structure of this paper is outlined as follows, in Section II, the models and corresponding rate equations of the RNI network and RNH network based on NLs are presented in detail. In Section III, we conduct a detailed study of the TDS hiding performance in the RNI network and RNH network by introducing the ACF. Specifically, we investigate how system parameters such as coupling strength, frequency detuning, Purcell factor F, spontaneous radiation coupling factor β, and bias current I affect the TDS of NLs in both networks. In addition, the impact of the coupling delay selection on the TDS concealment in RNH networks is discussed. Finally, we draw fundamental conclusions based on the results obtained in Section IV.

II. THEORY AND MODEL

The schematic illustrations of RNI network and RNH network are shown in Fig. 1. The system consists of three mutually coupled NLs systems. For the RNI network, the coupling delay is set to $\tau_{12} = \tau_{13} = \tau_{23} = \tau$. In contrast, for the RNH network, the coupling delay is $\tau_{12} = \tau$, $\tau_{13} = p\tau$, $\tau_{23} = q\tau$. The theoretical model of the RNH network system is mathematically formulated using mathematical methods [41], [43], as follows.

$$\begin{aligned}\frac{dS_m(t)}{dt} &= \Gamma\left[\frac{F\beta N_m(t)}{\tau_n} + \frac{g(N_m(t)-N_0)}{1+\varepsilon S_m(t)}S_m(t)\right] - \frac{1}{\tau_p}S_m(t) \\ &\quad + 2\sum_{n=1,n\neq m}^{3} kr_{nm}\sqrt{S_m(t)S_n(t-\tau_{nm})}\cos(\theta_{nm}(t)) \end{aligned} \tag{1}$$

$$\begin{aligned}\frac{dN_m(t)}{dt} &= \frac{I_m}{eV} - \frac{N_m(t)}{\tau_n}(F\beta+(1-\beta)) - \frac{g(N_m(t)-N_0)}{1+\varepsilon S_m(t)}S_m(t) \end{aligned} \tag{2}$$

$$\begin{aligned}\frac{d\phi_m(t)}{dt} &= \frac{\alpha}{2}\Gamma g(N_m(t)-Nth) - \left(2\pi\sum_{n=1,n\neq m}^{3}\Delta f_{nm}\right) \\ &\quad - \left(2\sum_{n=1,n\neq m}^{3} kr_{nm}\sqrt{\frac{S_n(t-\tau_{nm})}{S_m(t)}}\sin(\theta_{nm}(t))\right) \end{aligned} \tag{3}$$

$$\theta_{nm}(t) = -2\pi\Delta f_{mn}t + 2\pi f_n\tau_{mn} + \phi_m(t) - \phi_n(t-\tau_{mn}) \tag{4}$$

$$\theta_{mn}(t) = 2\pi\Delta f_{mn}t + 2\pi f_m\tau_{mn} + \phi_n(t) - \phi_m(t-\tau_{mn}) \tag{5}$$

where, the subscripts $m = 1,2,3$ and $n = 1,2,3$ represent the three NLs. $S(t)$represents the photon density, $N(t)$ is the carrier density, and $\emptyset(t)$ corresponds to the phase. τ_n and τ_p are the carrier lifetime and photon lifetime, respectively. F is the Purcell factor, and β is the spontaneous radiation coupling factor, both of which are critical parameters in NLs. Γ is the confinement factor, g is the differential gain, ε is the gain saturation factor, N_0 represents the transparency carrier density, and $Nth(Nth = N_0+1/\Gamma\tau_n g)$ denotes the threshold carrier density. The symbol e stands for the electron charge,

while V represents the active region volume, and I $(I{=}2Ith)$ stands for the bias current, where Ith signifies the threshold current. Furthermore, α denotes the linewidth enhancement factor, and Δf represents the frequency detuning between two NLs.

It should be noted that the final term in (1) and (3) represents mutual coupling, where kr_{mn} represents the coupling strength, and τ_{mn} denotes the coupling delay. For the shake of simplicity, we consider $kr_{mn} = kr_{nm} = kr$ and $\tau_{mn} = \tau_{nm} = \tau$ unless otherwise stated. On the other hand, it is worth noting that when the frequency detuning Δf_{mn} is not the same, the phase change for each injection path is different. Therefore, $\theta_{mn}(t)$ and $\theta_{nm}(t)$ are numerically distinct, and the expressions for the two phases are given in (4) and (5). Additionally, the formula for calculating kr is given by [40], where R_{inj} is the injection ratio, R is the cavity facet reflectivity of the NLs, c denotes the speed of light, n stands for the refractive index, and L represents the length of the feedback cavity.

$$kr = (1 - R)\sqrt{\frac{R_{inj}}{R}}\frac{c}{2nL} \tag{6}$$

In the study of this paper, we utilize the fourth-order Runge-Kutta scheme for numerical solutions of (1)-(5). The noise term is neglected in the simulations. Table 1 lists the values of several crucial parameters employed in the simulations.

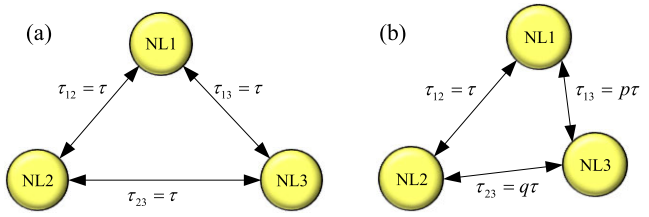

FIGURE 1. The schematic illustrations of ring networks. (a): the RNI network; (b): the RNH network. NL1: the first nano-laser; NL2: the second nano-laser; NL3: the third nano-laser.

TABLE 1. Parameters employed for the numerical simulations [43].

Parameter	Description	Value
Γ	confinement factor	0.645
τ_n	carrier lifetime	1 *ns*
τ_p	photon lifetime	0.36 *ps*
g	differential gain	1.64×10^{-6} cm^3/s
N_0	transparency carrier density	1.1×10^{18} cm^{-3}
ε	gain saturation factor	2.3×10^{-17} cm^3
α	linewidth enhancement factor	5
V	volume of active region	3.96×10^{-13} cm^3
λ_0	wavelength of NL	1591 *nm*
R	laser facet reflectivity	0.85
R_{inj}	injection ratio	0–0.1
n	refractive index	3.4
L	cavity length	1.39 μm
Q	quality factor	428

To quantify TDS numerically, we employ the effective ACF [41]. Throughout subsequent sections of this research, we consider that TDS is better concealed when the ACF peak is below 0.2. The ACF function is expressed by the following equation:

$$C(\Delta t) = \frac{\langle [I(t+\Delta t) - \langle I(t+\Delta t)\rangle][I(t) - \langle I(t)\rangle]\rangle}{\sqrt{\langle [I(t+\Delta t) - \langle I(t+\Delta t)\rangle]^2\rangle \langle [I(t) - \langle I(t)\rangle]^2\rangle}} \tag{7}$$

where $< >$ represents the average value of a time series, and Δt is the lag time.

III. RESULTS AND DISCUSSION

In this section, we initially illustrate the TDS characteristics of the RNI network and RNH network through the analysis of time series, power spectrum, and ACF plots. Subsequently, the influence of coupling strength, frequency detuning, Purcell factor F, spontaneous radiation coupling factor β and bias current I on the TDS concealment performance are analyzed in detail. Finally, the effects of different p and q selections in RNH networks on TDS are discussed.

Firstly, we present the time series, power spectrum, and ACF plots of the RNI network, as shown in Fig. 2. Here, we consider $F = 14$, $\beta = 0.05$, $I{=}2Ith$, $Ith = 1.1$mA, $\Delta f_{12} = \Delta f_{13}{=}0$GHz, and the coupling strength and coupling delay are symmetric, i.e., $kr_{12} = kr_{13} = kr_{23} = kr = 50\text{ns}^{-1}$, $\tau_{12} = \tau_{13} = \tau_{23} = \tau{=}0.5$ns. From Fig. 2(a1, b1, c1), it can be observed that all three NLs in the network operate in a chaotic state, and time sequences have noise-like waveforms and do not see the obvious characteristic information. However, when ACF characterizes correlated information, it is found that additional peaks are evident at coupling delays $\Delta t = 0.5$ns, $\Delta t = 1$ns and their multiples, as shown in Fig. 2(a3, b3, c3). In addition, the power spectrum exhibits distinct frequency spaces, indicating information leakage and

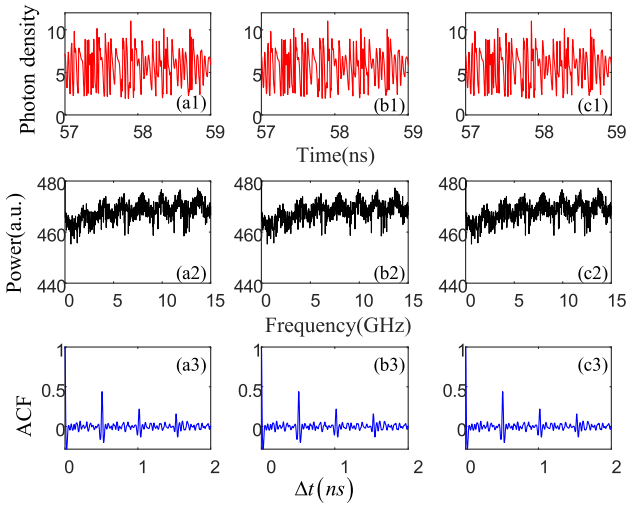

FIGURE 2. (a1, b1, c1): The time-series plots (in red), (a2, b2, c2): power spectrum (in black) and (a3, b3, c3): ACF (in blue) of the chaotic signals from three NLs. (a1, a2, a3): NL1, (b1, b2, b3): NL2, (c1, c2, c3): NL3. $\Delta f_{12} = \Delta f_{13}{=}0$GHz, $kr_{12}{=}kr_{13}{=}kr_{23}{=}kr{=}50\text{ns}^{-1}$, $\tau_{12} = \tau_{13} = \tau_{23} = \tau{=}0.5$ns, $F{=}14$, $\beta{=}0.05$, $I{=}2Ith$, $Ith{=}1.1$mA.

further confirming that the NLs in the RNI network under the specified parameters cannot conceal TDS.

To directly compare the RNI and RNH networks, Fig. 3 illustrates the outputs of the three NLs in the RNH network, where the parameters are consistent with those in Fig. 2 except that the coupling delay is randomly chosen as $\tau_{12} = \tau$, $\tau_{13} = 1.1\tau$, and $\tau_{23} = 0.8\tau$. Interestingly, the results in Fig. 3 show significant changes in the power spectrum and ACF plots by intentionally introducing asymmetric coupling delays. It can be seen from the Fig. 3 that the power spectrum becomes very flat with no obvious peak spacing visible and no obvious peaks around the delay, which indicates that the TDS is completely concealed. From a physical phenomenon perspective, this is because the network introduces additional nonlinearity and complexity, which can increase the system's randomness, making it more difficult to be observed. Therefore, in contrast to the RNI network, the RNH network demonstrates a substantial enhancement in concealing TDS.

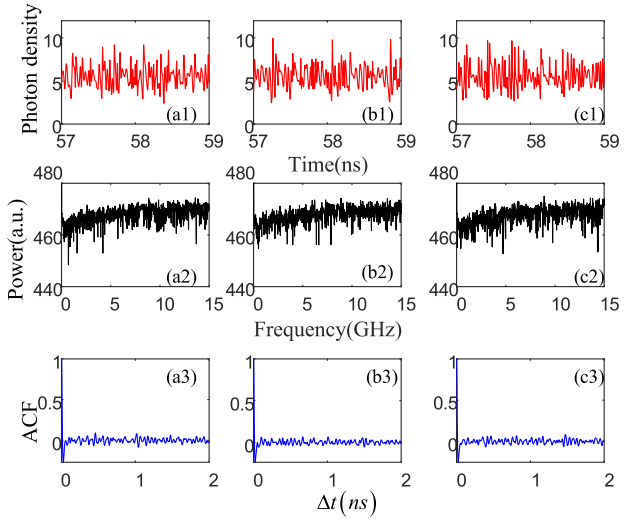

FIGURE 3. (a1, b1, c1): The time-series plots (in red), (a2, b2, c2): power spectrum (in black) and (a3, b3, c3): ACF (in blue) of the chaotic signals from three NLs. (a1, a2, a3): NL1, (b1, b2, b3): NL2, (c1, c2, c3): NL3. $\tau_{12} = \tau$, $\tau_{13} = 1.1\tau$, $\tau_{23} = 0.8\tau$. Other parameters are identical to those in Figure 2.

Next, to further observe the TDS concealment performance in the outputs of NLs within the RNI network and the RNH network, Fig. 4 is given. The figure's horizontal axis denotes frequency detuning Δf_{12}, with the vertical axis indicating coupling strength kr. The areas characterized by an ACF value below 0.2 (depicted in deep blue) indicate better TDS concealment. From the Fig. 4, it can be seen that the TDS evolution patterns of the three NLs are similar. For the RNI network, to enhance clarity, we label the parameter region below 0.2 as "L". From Fig. 4(a1, a2, a3), it is evident that the "L" regions in the three NLs are symmetric about $\Delta f_{12} = 0$GHz. Consequently, regions characterized by higher ACF values are predominantly found at the lower end for low coupling strength kr and at the top for high kr near $\Delta f_{12} = 0$GHz. Moreover, for this RNI network, NLs cannot

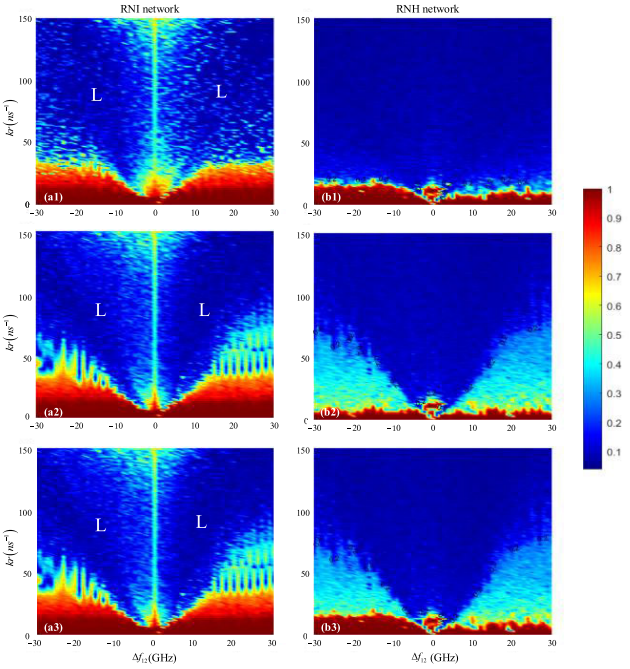

FIGURE 4. Two-dimensional plots of ACF values in the (Δf_{12}, kr) plane for the chaotic outputs of the three NLs in the RNI network (left column) and the RNH network (right column). (a1, b1): NL1; (a2, b2): NL2; (a3, b3): NL3. kr_{mn}=kr_{nm}=kr, Δf_{13}=0GHz, F=14, β=0.05, I=2Ith, Ith=1.1mA.

achieve TDS concealment at $\Delta f_{12} = 0$GHz regardless of the value of kr. It should be noted that this characteristic stands in stark contrast to the conventional system involving two mutually coupled NLs, where a "V"-like region indicating low TDS can be numerically discerned within the identical injection parameter plane [43]. Therefore, in comparison to mutually coupled NLs systems, the low TDS region of this RNI network is significantly expanded, allowing for wide-ranging tuning of frequency detuning. Furthermore, it is readily apparent that for the RNH network, the parameter region in which NLs achieve TDS concealment is larger than that of the RNI network, as shown in Fig. 4(b1, b2, b3). In this network, as kr increases gradually, the hiding effect of TDS becomes better, while the influence of Δf_{12} on TDS is minor, which contrasts sharply with the RNI network. These results confirm that the RNH network has higher complexity, thereby achieving better TDS hiding.

There have been studies proving that F, β, and I significantly affect the dynamical characteristics of NLs. Here, we first investigate the variation of the TDS values of NLs in two different networks under various conditions of F and β, as shown in the line graph in Fig. 5. From this figure, it can be observed that for $F = 14$ and $\beta = 0.05$, the ACF value of the RNH network is significantly lower than that of the RNI network at the equivalent coupling strength. Furthermore, when $kr > 25\text{ns}^{-1}$, the ACF value of the RNH network is less than 0.2 and tends to stabilize, while the ACF of the RNI network is consistently greater than 0.2 over the entire coupling strength range, which indicates that, compared to

the RNI, the RNH network can achieve TDS hiding across a larger range of parameters. For $F = 14$ and $\beta = 0.1$, the ACF curve of the RNI network is significantly shifted up a little bit compared to that of $F = 14$ and $\beta = 0.05$, i.e., the value of ACF increases. Similarly, a similar phenomenon occurs in the RNH network, especially in the ranges $22\text{ns}^{-1} < kr < 36\text{ns}^{-1}$, $59\text{ns}^{-1} < kr < 69\text{ns}^{-1}$, and $92\text{ns}^{-1} < kr < 99\text{ns}^{-1}$, as shown in Fig. 5(b1, b2, b3). The reason for this phenomenon is that the increase of β from 0.05 to 0.1 enhances the damping of the relaxation oscillations of NLs. The more intense the damping of relaxation oscillations, the better the stability, leading to an increase in the peak value of ACF. Although the ACF values of both networks increase in this case, the ACF value of the RNH network is still much smaller compared to the RNI network. Finally, when F is increased to 30, i.e., $F = 30$ and $\beta = 0.1$, it can be seen from Fig. 5(c1, c2, c3) that the trend of the ACF curve of the RNI network is similar to the previous two cases, but the ACF values increase again. At the same time, the ACF value of the RNH network also significantly increases. This phenomenon arises from the heightened damping of NLs' relaxation oscillations due to the increased values of F and β. In general, as F and β increase, the range of TDS concealment in both the RNH and RNI networks decreases. From a physical perspective, this variation is caused by the damping of relaxation oscillations. However, the area where NLs achieve TDS concealment in the RNH network is much larger than in the RNI network. On the other hand, we observe that the ACF curve of the RNH network undergoes significant and irregular changes, even exceeding the ACF values of the RNI network in some coupling strength ranges. This phenomenon is quite interesting and suggests that the TDS evolution in the RNH network exhibits greater complexity, potentially linked to the non-resonant heating effect [44].

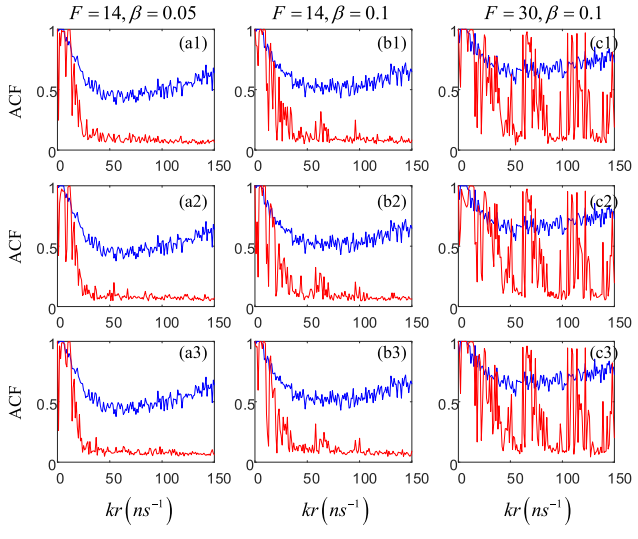

FIGURE 5. The relationship between the peak values of ACF for three NLs and the coupling strength under different values of F and β in the RNI network (blue curve) and the RNH network (red curve). NL1: the first row; NL2: the second row; NL3: the third row. (a1, a2, a3): F=14, β=0.05; (b1, b2, b3): F=14, β=0.1; (c1, c2, c3): F=30, β=0.1. I=2Ith, Ith=1.1mA, $\Delta f_{12} = \Delta f_{13}$=0GHz.

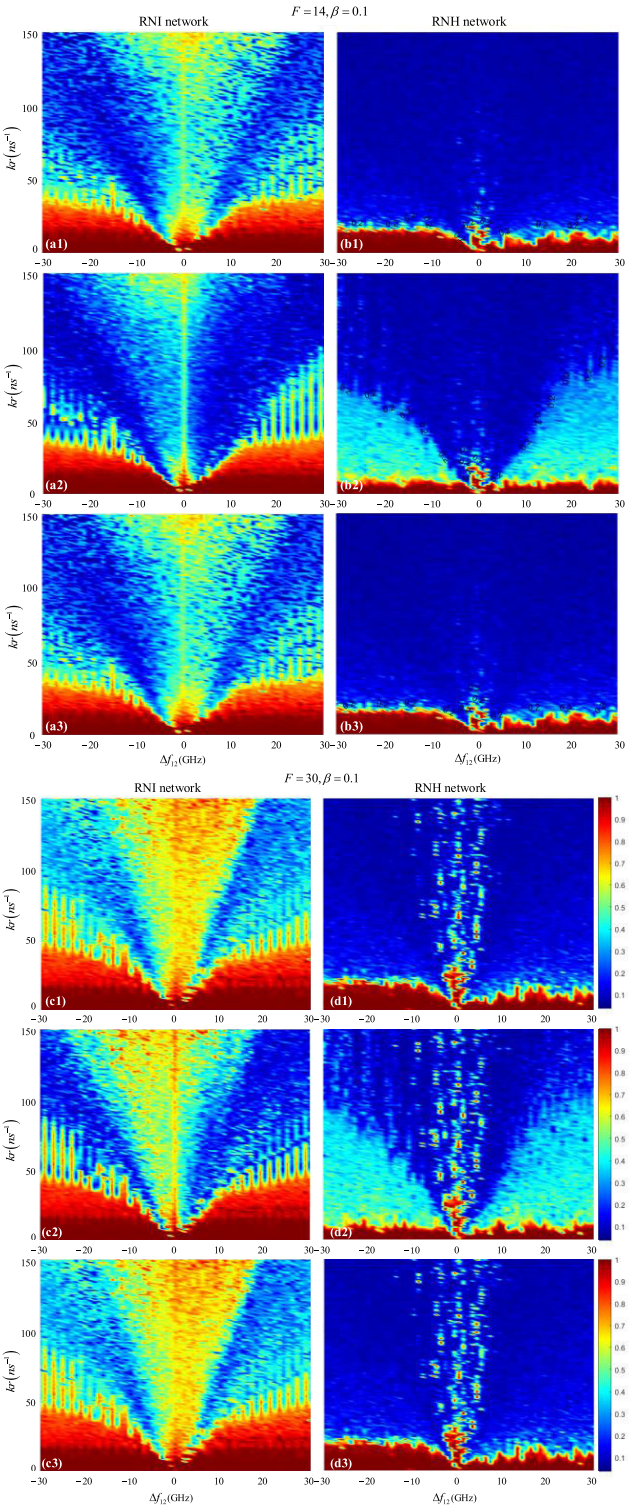

FIGURE 6. Two-dimensional plots of ACF values in the (Δf_{12}, kr) plane for the chaotic outputs of the three NLs for different values of F and β in the RNI network and the RNH network. (a1, b1, c1, d1): NL1; (a2, b2, c2, d2): NL2; (a3, b3, c3, d3): NL3. The RNI network: (a1, a2, a3) and the RNH network: (b1, b2, b3) under F=14, β=0.1; The RNI network: (c1, c2, c3) and the RNH network: (d1, d2, d3) under F=30, β=0.1. kr_{mn}=kr_{nm}=kr, Δf_{13}=0GHz, I=2Ith, Ith=1.1mA.

Subsequently, a further quantitative evaluation of the influence of F and β on TDS in the RNI network and the RNH network was conducted. The two-dimensional mapping of ACF peak values in the frequency detuning and coupling strength parameter space is shown in Fig. 6. Here, we compare Figs. 4 and 6 because the only differences between them are the values of F and β. Three sets of data are considered: $F = 14$, $\beta = 0.05$, $F = 14$, $\beta = 0.1$ and $F = 30$, $\beta = 0.1$. Firstly, observing the RNI network, it can be seen from Figs. 4(a1, a2, a3) and 6(a1, a2, a3) (c1, c2, c3) that as F and β values increase, the "L" region gradually shrinks.

This indicates that the region where TDS is concealed decreases, as larger F and β values result in increased damping of relaxation oscillations, and the more pronounced the damping of relaxation oscillations, the better the stability, leading to a reduction in the hidden TDS region. Additionally, it is observed that the ACF values in the RNI network are closely related to kr and Δf_{12}. With increasing F and β, the tunable range of kr and Δf_{12} becomes smaller. Next, we observe the RNH network. When $F = 14$ and β=0.1, the TDS hidden region depicted in Fig. 6(b1, b2, b3) is similar to that in Fig. 4(b1, b2, b3) since F remains constant and β only slightly increases. Nevertheless, with $F = 30$ and β=0.1, Fig. 6(d1, d2, d3) illustrates the TDS concealed region significantly decreases, mainly in the scope of Δf_{12} =(−10GHz,10GHz). In summary, for improved concealment of TDS in NLs over a broader parameter range, it is suggested to employ NLs characterized by moderate F and smaller β. Moreover, unlike the RNI network, the RNH network demonstrates the capability to achieve TDS concealment across a broader range of parameters. These conclusions are consistent with those in Fig. 5.

Since the bias current I is another key parameter in the NLs, we present the ACF line plots of NL1 (the results for the three NLs are extremely similar) in the two networks at different I values with varying kr, as shown in Fig. 7. In the RNI network (dotted lines), it is clear from the plots that as the current Igradually increases, the ACF values decrease

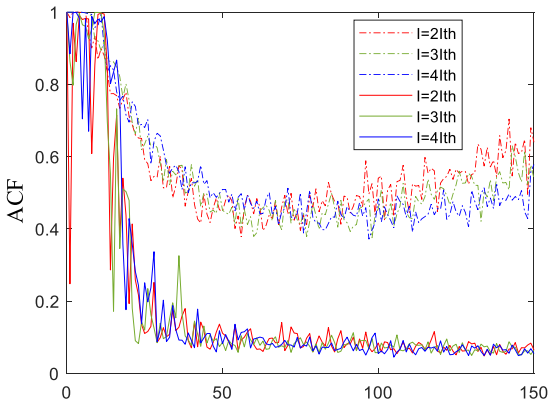

FIGURE 7. The relationship between the peak values of ACF for NL1 and the coupling strength under different values of I in the RNI network (dotted lines) and the RNH network (solid lines). The red: I=2Ith; The green: I=3Ith; The blue: I=4Ith. F=14, β=0.05. $\Delta f_{12} = \Delta f_{13}$=0GHz.

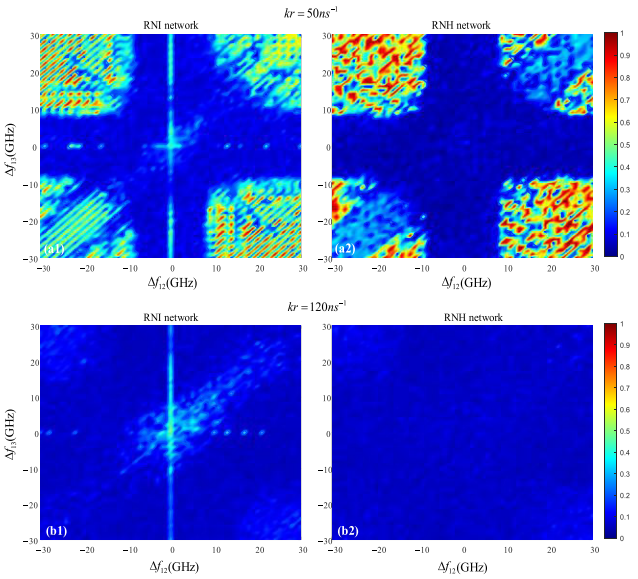

FIGURE 8. Two-dimensional plots of ACF values in the (Δf_{12}, Δf_{13}) plane for the chaotic outputs of the NL1 for coupling strength kr in the RNI network (left column) and the RNH network (right column). (a1, a2): kr=50ns^{-1}; (b1, b2): kr=120ns^{-1}. F=14, β=0.05, I=2Ith, Ith=1.1mA.

with the increase of kr, which indicates that larger injection currents are required to suppress the TDS. Conversely, in the case of the RNH network, the variation in ACF is minimal with increasing I, especially in the range of $kr > 40\text{ns}^{-1}$, maintaining consistently very low ACF values, significantly lower than those of the RNI network. These results show that large currents I can reduce the ACF values in the RNI network, while their impact on the RNH network is minimal. In particular, a large current I can effectively conceal the TDS of the RNI network across a broader range, with minimal impact on hiding TDS in the RNH network.

For all the results obtained above, only the frequency detuning between two NLs was considered, and Δf_{12} has a larger effect on TDS. In order not to lose the generality, the next step is to study the frequency detuning among three NLs. From the previous studies, it can be seen that the TDS characteristics of the outputs of the three NLs are similar. Therefore, we focus only on the study of NL1 here. Fig. 8 shows the ACF values of NL1 in the RNI network and RNH network under different coupling strengths kr, with the horizontal axis Δf_{12} and the vertical axis Δf_{13}. When kr=50ns^{-1}, it can be observed from Fig. 8(a1, a2) that Δf_{12} and Δf_{13} have a significant impact on both types of ring networks, and TDS concealment cannot be achieved at the four corners of the entire plane, with parameter ranges being $\Delta f_{12} = [-30, -10]$ and $\Delta f_{13} = [-30, -10]$, $\Delta f_{12} = [-30, -10]$ and $\Delta f_{13} = [10, 30]$, $\Delta f_{12} = [10, 30]$ and $\Delta f_{13} = [-30, -10]$, and $\Delta f_{12} = [10, 30]$ and $\Delta f_{13} = [10, 30]$. It is noteworthy that the RNI network cannot achieve TDS concealment at $\Delta f_{12} = 0$GHz and $\Delta f_{13} = 0$GHz, while the RNH network has no impact at 0GHz. When kr is a larger value, 120ns^{-1} in this case, the RNI network fails

to achieve TDS concealment near $\Delta f_{12} = 0$GHz and $\Delta f_{13} = 0$GHz, while the RNH network exhibits the ability to achieve TDS hiding across the entire parameter spectrum, as shown in Fig. 8(b1, b2). In summary, the region where the RNH network achieves TDS concealment is larger than that of the RNI network, and these findings further validate the previous results.

Finally, without losing generality, we also explore additional coupling delays and give Fig. 9. Fig. 9 depicts the two-dimensional mapping of the ACF peak values of the three NLs in the q and p parameter space under different coupling strengths kr, where we consider $\tau_{12} = \tau$, $\tau_{13} = p\tau$ and $\tau_{23} = q\tau$. From Fig. 9(a1, a2, a3), it is apparent that when kr=50ns^{-1}, the NLs can obtain lower ACF values in most of the parameter ranges, i.e., TDS concealment is achieved. However, there are a few specific lines within the parameter realm of p and q where some ACF values are slightly higher, such as $p = 1$, $q = 1$, $p + q = 0.8$, and $p = q$. This implies a potential correlation between the effectiveness of TDS concealment in the RNH network and the choice of coupling delays. On the other hand, when the coupling strength is higher, kr=120ns^{-1}, the ACF values are relatively low across the entire parameter range. Therefore, the robustness of TDS hiding can be enhanced by using a larger coupling strength. This result can provide recommendat- ions for obtaining better TDS concealment in RNH networks.

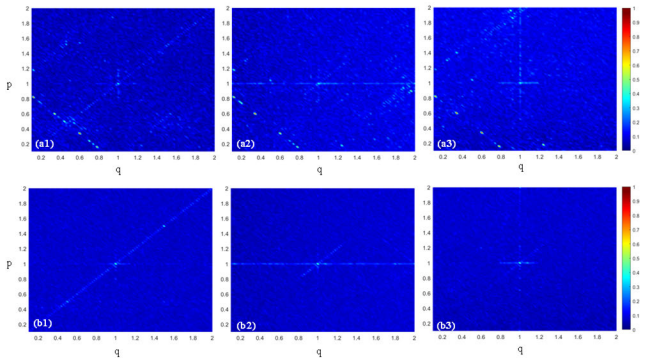

FIGURE 9. Two-dimensional plots of ACF values in the (p, q) plane for the chaotic outputs of the three NLs for coupling strength kr in the RNH network. (a1, a2, a3): kr=50ns^{-1}; (b1, b2, b3): kr=120ns^{-1}; The first column: NL1, the second column: NL2, the third column: NL3. $\tau_{12} = \tau$, $\tau_{13} = p\tau$, $\tau_{23} = q\tau$. F=14, β =0.05, I=2Ith, Ith=1.1mA, $\Delta f_{12} = \Delta f_{13} = 0$GHz.

IV. CONCLUSION

In summary, in this paper, the TDS characteristics of NLs output chaos in this structure are numerically investigated based on the single-mode rate equations of NLs and intentionally the introduction of heterogeneous coupling delays in the ring network. The focus of this study is on investigating the effects of coupling strength, frequency detuning, Purcell factor F, spontaneous radiation coupling factor β, and bias current I on TDS concealment. The results indicate that, compared to ring networks with the identical coupling delay, ring networks with heterogeneous delays can better conceal TDS. In addition, moderate F and smaller β value enable TDS hiding across a larger range of coupling intensity and frequency detuning, while I has a relatively minor impact on TDS in ring networks with heterogeneous delays. Finally, by plotting the evolution of ACF values in the output of NLs in a ring network with heterogeneous delays against the delay selection, it is found that ACF values are consistently low across almost the entire parameter space. Moreover, adopting a larger coupling strength enhances the robustness of TDS concealment. Therefore, this research provides a theoretical basis for the application of other network topologies composed of novel NLs to achieve higher security in subsequent studies.

REFERENCES

[1] D. Wang, L. Wang, P. Li, T. Zhao, Z. Jia, Z. Gao, Y. Guo, Y. Wang, and A. Wang, "Bias current of semiconductor laser: An unsafe key for secure chaos communication," *Photonics*, vol. 6, no. 2, p. 59, May 2019, doi: 10.3390/photonics6020059.

[2] X. Zhang, P. Mu, G. Guo, X. Liu, and P. He, "Bidirectional chaotic synchronization communication of closed-loop mutually coupled nano-lasers," *Electronics*, vol. 13, no. 1, p. 239, Jan. 2024, doi: 10.3390/electronics13010239.

[3] Y. Tang, Q. Li, W. Dong, M. Hu, and R. Zeng, "Optical chaotic communication using correlation demodulation between two synchronized chaos lasers," *Opt. Commun.*, vol. 498, Nov. 2021, Art. no. 127232, doi: 10.1016/j.optcom.2021.127232.

[4] S. Xiang, B. Wang, Y. Wang, Y. Han, A. Wen, and Y. Hao, "2.24-Tb/s physical random bit generation with minimal post-processing based on chaotic semiconductor lasers network," *J. Lightw. Technol.*, vol. 37, no. 16, pp. 3987–3993, Aug. 2019.

[5] S. Zhang, X. Tang, G.-Q. Xia, and Z.-M. Wu, "Fast physical random bit generation based on an optoelectronic delay loop pumped by a semiconductor laser under a modulated optical feedback," *Proc. SPIE*, vol. 11545, Oct. 2020, doi: 10.1117/12.2575242.

[6] J. D. Hart, Y. Terashima, A. Uchida, G. B. Baumgartner, T. E. Murphy, and R. Roy, "Recommendations and illustrations for the evaluation of photonic random number generators," *APL Photon.*, vol. 2, no. 9, Aug. 2017, Art. no. 090901, doi: 10.1063/1.5000056.

[7] B. Liu, Y. Jiang, and H. Ji, "Sensing by dynamics of lasers with external optical feedback: A review," *Photonics*, vol. 9, no. 7, p. 450, Jun. 2022, doi: 10.3390/photonics9070450.

[8] E. A. Yarunova, A. A. Krents, N. E. Molevich, and D. A. Anchikov, "Suppression of spatiotemporal instabilities in broad-area lasers with pump modulation by external optical injection," *Bull. Lebedev Phys. Inst.*, vol. 48, no. 2, pp. 55–58, Feb. 2021, doi: 10.3103/s1068335621020081.

[9] P. S. Dmitriev, A. V. Kovalev, A. Locquet, D. S. Citrin, E. A. Viktorov, and D. Rontani, "Predicting chaotic time series using optoelectronic feedback laser," *Proc. SPIE*, vol. 11356, Apr. 2020, Art. no. 113560U, doi: 10.1117/12.2556368.

[10] O. Spitz, J. Wu, A. Herdt, M. Carras, W. Elsäßer, C.-W. Wong, and F. Grillot, "Investigation of chaotic and spiking dynamics in mid-infrared quantum cascade lasers operating continuous-waves and under current modulation," *IEEE J. Sel. Topics Quantum Electron.*, vol. 25, no. 6, pp. 1–11, Nov. 2019, doi: 10.1109/JSTQE.2019.2937445.

[11] A. Elsonbaty, S. F. Hegazy, and S. S. A. Obayya, "Simultaneous concealment of time delay signature in chaotic nanolaser with hybrid feedback," *Opt. Lasers Eng.*, vol. 107, pp. 342–351, Aug. 2018, doi: 10.1016/j.optlaseng.2018.03.027.

[12] H. Liu, B. Ren, Q. Zhao, and N. Li, "Characterizing the optical chaos in a special type of small networks of semiconductor lasers using permutation entropy," *Opt. Commun.*, vol. 359, pp. 79–84, Jan. 2016, doi: 10.1016/j.optcom.2015.09.059.

[13] D. Rontani, A. Locquet, M. Sciamanna, D. S. Citrin, and S. Ortin, "Time-delay identification in a chaotic semiconductor laser with optical feedback: A dynamical point of view," *IEEE J. Quantum Electron.*, vol. 45, no. 7, pp. 879–1891, Jul. 2009, doi: 10.1109/JQE.2009.2013116.

[14] R. M. Nguimdo, P. Colet, L. Larger, and L. Pesquera, "Digital key for chaos communication performing time delay concealment," *Phys. Rev. Lett.*, vol. 107, no. 3, Jul. 2011, Art. no. 034103, doi: 10.1103/physrevlett.107.034103.

[15] A. Uchida, K. Amano, M. Inoue, K. Hirano, S. Naito, H. Someya, I. Oowada, T. Kurashige, M. Shiki, S. Yoshimori, K. Yoshimura, and P. Davis, "Fast physical random bit generation with chaotic semiconductor lasers," *Nature Photon.*, vol. 2, no. 12, pp. 728–732, Dec. 2008, doi: 10.1038/nphoton.2008.227.

[16] A. Zhao, N. Jiang, S. Liu, C. Xue, and K. Qiu, "Wideband time delay signature-suppressed chaos generation using self-phase-modulated feedback semiconductor laser cascaded with dispersive component," *J. Lightw. Technol.*, vol. 37, no. 19, pp. 5132–5139, Oct. 2019.

[17] J.-G. Wu, G.-Q. Xia, and Z.-M. Wu, "Suppression of time delay signatures of chaotic output in a semiconductor laser with double optical feedback," *Opt. Exp.*, vol. 17, no. 22, pp. 20124–20133, Oct. 2009, doi: 10.1364/oe.17.020124.

[18] J.-G. Wu, Z.-M. Wu, J.-T. Shen, L. Ding, N.-Y. Li, and G.-Q. Xia, "Suppression of time delay signatures of chaotic output in mutually delay-coupled semiconductor lasers," *Proc. SPIE*, vol. 7844, pp. 47–52, Nov. 2010, doi: 10.1117/12.869959.

[19] P. Mu, W. Pan, L. Yan, B. Luo, and X. Zou, "Concealment of chaos time-delay signature through phase-conjugate feedback and chaos optical injection," *IEEE Photon. J.*, vol. 9, no. 5, pp. 1–8, Oct. 2017, doi: 10.1109/JPHOT.2017.2754410.

[20] Y. Ma, S. Xiang, X. Guo, Z. Song, A. Wen, and Y. Hao, "Time-delay signature concealment of chaos and ultrafast decision making in mutually coupled semiconductor lasers with a phase-modulated Sagnac loop," *Opt. Exp.*, vol. 28, no. 2, pp. 1665–1678, Jan. 2020, doi: 10.1364/oe.384378.

[21] P. Zhou, Q. Fang, and N. Li, "Phased-array assisted time-delay signature suppression in the optical chaos generated by an external-cavity semiconductor laser," *Opt. Lett.*, vol. 45, no. 2, pp. 399–402, Jan. 2020, doi: 10.1364/ol.381782.

[22] T. Mihana, K. Fujii, K. Kanno, M. Naruse, and A. Uchida, "Laser network decision making by lag synchronization of chaos in a ring configuration," *Opt. Exp.*, vol. 28, no. 26, pp. 40112–40130, Dec. 2020, doi: 10.1364/oe.411140.

[23] S. Liu, N. Jiang, A. Zhao, Y. Zhang, and K. Qiu, "Secure optical communication based on cluster chaos synchronization in semiconductor lasers network," *IEEE Access*, vol. 8, pp. 11872–11879, 2020, doi: 10.1109/ACCESS.2020.2965960.

[24] M. Bourmpos, A. Argyris, and D. Syvridis, "Sensitivity analysis of a star optical network based on mutually coupled semiconductor lasers," *J. Lightw. Technol.*, vol. 30, no. 16, pp. 2618–2624, Aug. 2012.

[25] S. Xiang, A. Wen, and W. Pan, "Synchronization regime of star-type laser network with heterogeneous coupling delays," *IEEE Photon. Technol. Lett.*, vol. 28, no. 18, pp. 1988–1991, Sep. 2016, doi: 10.1109/LPT.2016.2581310.

[26] L. Zhang, W. Pan, L. Yan, B. Luo, X. Zou, and M. Xu, "Isochronous cluster synchronization in delay-coupled VCSEL networks subjected to variable-polarization optical injection with time delay signature suppression," *Opt. Exp.*, vol. 27, no. 23, pp. 33369–33377, Nov. 2019, doi: 10.1364/oe.27.033369.

[27] N. Li, W. Pan, S. Xiang, L. Yan, B. Luo, and X. Zou, "Loss of time delay signature in broadband cascade-coupled semiconductor lasers," *IEEE Photon. Technol. Lett.*, vol. 24, no. 23, pp. 2187–2190, Dec. 2012, doi: 10.1109/LPT.2012.2225101.

[28] H. Liu, N. Li, and Q. Zhao, "Photonic generation of polarization-resolved wideband chaos with time-delay concealment in three-cascaded vertical-cavity surface-emitting lasers," *Appl. Opt.*, vol. 54, no. 14, pp. 4380–4387, May 2015, doi: 10.1364/ao.54.004380.

[29] S. Xiang, A. Wen, W. Pan, L. Lin, H. Zhang, H. Zhang, X. Guo, and J. Li, "Suppression of chaos time delay signature in a ring network consisting of three semiconductor lasers coupled with heterogeneous delays," *J. Lightw. Technol.*, vol. 34, no. 18, pp. 4221–4227, Sep. 2016.

[30] J. Mork and G. L. Lippi, "Rate equation description of quantum noise in nanolasers with few emitters," *Appl. Phys. Lett.*, vol. 112, no. 14, Apr. 2018, Art. no. 141103, doi: 10.1063/1.5022958.

[31] Z. Abdul Sattar and K. A. Shore, "External optical feedback effects in semiconductor nanolasers," *IEEE J. Sel. Topics Quantum Electron.*, vol. 21, no. 6, pp. 500–505, Nov. 2015, doi: 10.1109/JSTQE.2015.2409984.

[32] Z. A. Sattar and K. A. Shore, "Dynamics of nanolasers subject to optical injection and optical feedback," *Proc. SPIE*, vol. 12, pp. 38–47, Mar. 2016, doi: 10.1117/12.2208663.

[33] Z. A. Sattar, N. A. Kamel, and K. A. Shore, "Optical injection effects in nanolasers," *IEEE J. Quantum Electron.*, vol. 52, no. 2, pp. 1–8, Feb. 2016, doi: 10.1109/JQE.2015.2512591.

[34] Z. A. Sattar and K. A. Shore, "Phase conjugate feedback effects in nanolasers," *IEEE J. Quantum Electron.*, vol. 52, no. 4, pp. 1–8, Apr. 2016, doi: 10.1109/JQE.2016.2535339.

[35] H. Han and K. A. Shore, "Dynamical characteristics of nano-lasers subject to optical injection and phase conjugate feedback," *IET Optoelectron.*, vol. 12, no. 1, pp. 25–29, Feb. 2018, doi: 10.1049/iet-opt.2017.0058.

[36] H. Han and K. A. Shore, "Zero crosstalk regime direct modulation of mutually coupled nanolasers," *IEEE Photon. J.*, vol. 9, no. 4, pp. 1–12, Aug. 2017, doi: 10.1109/JPHOT.2017.2705433.

[37] H. Han and K. A. Shore, "Analysis of high-frequency oscillations in mutually-coupled nano-lasers," *Opt. Exp.*, vol. 26, no. 8, pp. 10013–10022, Apr. 2018, doi: 10.1364/oe.26.010013.

[38] H. Han and K. A. Shore, "Modulated mutually coupled nano-lasers," *IEEE J. Quantum Electron.*, vol. 53, no. 2, pp. 1–8, Apr. 2017, doi: 10.1109/JQE.2017.2670542.

[39] B. Romeira and A. Fiore, "Purcell effect in the stimulated and spontaneous emission rates of nanoscale semiconductor lasers," *IEEE J. Quantum Electron.*, vol. 54, no. 2, pp. 1–12, Apr. 2018, doi: 10.1109/JQE.2018.2802464.

[40] Y. Qu, S. Xiang, Y. Wang, L. Lin, A. J. Wen, and Y. Hao, "Concealment of time delay signature of chaotic semiconductor nanolasers with double chaotic optical injections," *IEEE J. Quantum Electron.*, vol. 55, no. 2, pp. 1–7, Apr. 2019, doi: 10.1109/JQE.2019.2898673.

[41] P. Jiang, P. Zhou, N. Li, P. Mu, and X. Li, "Optically injected nanolasers for time-delay signature suppression and communications," *Opt. Exp.*, vol. 28, no. 18, pp. 26421–26435, Aug. 2020, doi: 10.1364/oe.403021.

[42] P. Jiang, P. Zhou, N. Li, P. Mu, and X. Li, "Characterizing the chaotic dynamics of a semiconductor nanolaser subjected to FBG feedback," *Opt. Exp.*, vol. 29, no. 12, pp. 17815–17830, Jun. 2021, doi: 10.1364/oe.427541.

[43] X. Zhang, G. Guo, X. Liu, G. Hu, K. Wang, and P. Mu, "Dynamics and concealment of time-delay signature in mutually coupled nano-laser chaotic systems," *Photonics*, vol. 10, no. 11, p. 1196, Oct. 2023, doi: 10.3390/photonics10111196.

[44] A. Wang, B. Wang, L. Li, Y. Wang, and K. A. Shore, "Optical heterodyne generation of high-dimensional and broadband white chaos," *IEEE J. Sel. Topics Quantum Electron.*, vol. 21, no. 6, pp. 531–540, Nov. 2015, doi: 10.1109/JSTQE.2015.2427253.

XUETING ZHANG received the bachelor's degree in communication engineering from Suqian University, in 2022. She is currently pursuing the master's degree in electronic information with Yantai University. Her current research interests include nonlinear dynamics of semiconductor nano-lasers, chaotic security communication, and photonic neurons.

PENGHUA MU (Member, IEEE) received the B.S. degree in communication engineering and the Ph.D. degree in optoelectronics from Southwest Jiaotong University, China, in 2009 and 2016, respectively. He joined the Institute of Science and Technology for Opto-Electronic Information, Yantai University. His current research interests include nonlinear dynamics of semiconductor lasers, random number generation, and chaotic security communication.

YIQIAO WANG received the B.S. degree in communication engineering from Yantai University, Shandong, in 2023, where she is currently pursuing the master's degree with the School of Physics and Electronic Information. Her current research interests include nonlinear dynamics of semiconductor lasers and photonic neurons.

GANG GUO was born in Weihai, Shandong, in 1966. He received the master's degree in software engineering from Beijing Institute of Technology.

He is currently the Chairperson and the General Manager of Fisherman Information Technology Company Ltd. He is also a Senior Engineer. To date, he has been granted eight national invention patents and three utility model patents. He is also the Head of the Cryptography Application Group of the National Information Innovation Work Committee, an Expert Member of the National Standardization Technical Committee for the Cryptography Industry, the Vice Chairperson of Shandong Commercial Cryptography Association, and a Mentor at the postdoctoral research and workstation. He has been awarded the honorary titles of ''Taishan Industry Leading Talent'' and ''Outstanding Software Entrepreneur'' in Shandong Province and the ''Blue Wisdom Double Hundred Talents'' in Shandong Peninsula National Independent Innovation Demonstration Zone. He has won the third prize for scientific and technological progress in cryptography at the provincial and ministerial level twice and the third prize for science and technology in Shandong province twice.

XINTIAN LIU was born in August 1987. He received the degree in computer science and technology from Shandong University of Science and Technology. He is currently the Product Director of Fisherman Information Technology Company Ltd. He is also a Senior Engineer. He has been focusing on the field of cryptographic technology in the information security industry for more than ten years. He has won one National Cryptography Science and Technology Progress Award (7/9), been granted five invention patents, and published two SCI papers.

XIA LIU received the B.Eng. degree from Yantai University, Shandong, China, in 2010, the M.Sc. degree from China University of Petroleum, Shandong, in 2012, and the Ph.D. degree from Beijing University of Posts and Telecommunication, Beijing, China. She is currently with the School of Physics and Electronic Information, Yantai University, as a Lecturer. Her current research interests include cognitive networks, the Internet of Things, and future mobile communication systems.